Flow condensation in parallel micro-channels – Part 2: Heat transfer results and correlation technique

Sung-Min Kim, Issam Mudawar *

Boiling and Two-Phase Flow Laboratory (BTPFL) and Purdue University International Electronic Cooling Alliance (PUIECA), Mechanical Engineering Building, 585 Purdue Mall, West Lafayette, IN 47907-2088, USA

ARTICLE INFO

ABSTRACT

This second part of a two-part study concerns heat transfer characteristics for FC-72 condensing along parallel, square micro-channels with a hydraulic diameter of 1 mm, which were formed in the top surface of a solid copper plate. Heat from the condensing flow was rejected to a counter flow of water through channels brazed to the underside of the copper plate. The FC-72 condensation heat transfer coefficient was highest near the channel inlet, where the annual liquid film is thinnest. The heat transfer coefficient decreased along the micro-channel because of the film thickening and eventual collapse of the annular regime. Notable heat transfer enhancement was observed for annular flow regions of the micro-channel associated with interfacial waves. Comparing the present data to predictions of previous annular condensation heat transfer correlations shows correlations intended for macro-channels generally provide better predictions than correlations intended specifically for mini/micro-channels. A new condensation heat transfer coefficient correlation is proposed for annular condensation heat transfer in mini/micro-channels. The new correlation shows excellent predictive capability based on both the present FC-72 data and a large database for mini/micro-channel flows amassed from eight previous sources.

© 2011 Elsevier Ltd. All rights reserved.

1. Introduction

Modern technologies are demanding more effective schemes to tackle heat removal from very high power density devices. The vast majority of research articles addressing high-flux electronic cooling that have been written during the past three decades have been dedicated to heat extraction from the device itself rather than the heat rejection. This trend is driven by the assumption that a commercial condenser could always be sized to reject the heat from virtually any cooling system.

An increasing number of aerospace and defense applications are demanding the use of a thermal management system containing two separate cooling loops. A primary coolant absorbs the heat from the high-flux device inside a compact boiler, and rejects it via a compact condenser to a second coolant in a secondary cooling loop that carries the heat away to a remote commercial heat exchanger, where the heat is rejected to ambient air (or sea water for marine applications). As described by Lee and Mudawar [1,2], the secondary cooling loop could consist of a low-temperature refrigeration cycle. Using separate cooling loops decouples the performance of the boiler from that of the refrigeration cycle, enabling

the dissipation of much higher device heat fluxes than with an evaporator incorporated directly in the refrigeration loop.

While compact boiler designs such as those employing micro-channel heat sinks [1,2] or jet-impingement [3] have been successfully demonstrated for these applications, packaging requirements impose equally stringent constraints on the size of the primary loop's condenser. In fact, commercial condensers are often far too large for these applications. Developing a compact high-flux condenser is therefore a primary motivation for the present study.

Part 1 of this study [4] discussed the design of a condensation module featuring a series of micro-channels that are used to condense FC-72 by rejecting heat to a counter flow of water. Key to achieving high condensation heat transfer coefficients is to maintain annular flow over a large fraction of the micro-channel's length. This flow regime consists of a liquid film that sheathes the channel walls, driven by the shear force exerted by the vapor core. The film is extremely thin in the upstream region of the micro-channel where the annular regime is initiated, which yields very high condensation heat transfer coefficients. The heat transfer coefficient decreases along the stream-wise direction as the annular film gradually thickens and, especially, as the annular regime is replaced, in succession, by transition, slug, bubbly and single-phase liquid flow regimes. Recognizing the importance of annular flow, previous condensation studies have focused mostly on this particular regime e.g., [5–12].

---

* Corresponding author. Tel.: +1 765 494 5705; fax: +1 765 494 0539.
E-mail address: mudawar@ecn.purdue.edu (I. Mudawar).
URL: https://engineering.purdue.edu/BTPFL (I. Mudawar).

Nomenclature

c_p	specific heat at constant pressure
D	tube diameter
D_h	hydraulic diameter
f	Fanning friction factor
G	mass velocity
g	gravitational acceleration
H_{ch}	micro-channel height
H_t	distance between top thermocouple plane and base of micro-channels
h	enthalpy; heat transfer coefficient
h_{fg}	latent heat of vaporization
J	superficial velocity
k	thermal conductivity
L	length of micro-channel
M	number of data points
MAE	mean absolute error
m	fin parameter
$\dot{m}$	mass flow rate
N	number of micro-channels in condensation module
Nu	Nusselt number
P	pressure
P_{crit}	critical pressure
P_R	reduced pressure, $P_R = P/P_{crit}$
Pr	Prandtl number
q''	heat flux
q''_w	heat flux based on micro-channel's cooled perimeter
q''_{base}	heat flux based on total base area of micro-channel condenser
Re	Reynolds number
Su_g	Suratman number, $Su_g = \rho_g \sigma D / \mu_g^2$
T	temperature
T_b	temperature in bottom thermocouple plane in copper block
T_f	Fluid temperature
T_{sat}	fluid saturation temperature
T_t	temperature in top thermocouple plane in copper block
$T_{w,b}$	bottom-wall temperature of micro-channel

$T\delta^+$	dimensionless boundary layer temperature
u^*	friction velocity
v	specific volume
W_{ch}	micro-channel width
W_s	width of solid wall separating micro-channels
We	Weber number
We^*	modified Weber number
X	Martinelli parameter, $X = \sqrt{(dP/dz)_f / (dP/dz)_g}$
x	thermodynamic equilibrium quality
z	stream-wise coordinate

Greek Symbols

β	channel aspect ratio, W_{ch}/H_{ch}
η	fin efficiency
μ	dynamic viscosity
ρ	density
σ	surface tension
τ_w	wall shear stress
ϕ	two-phase pressure drop multiplier

Subscripts

3	based on three-sided heat transfer in rectangular channel
4	based on four-sided heat transfer in rectangular channel
cir	based on uniform circumferential cooling
exp	experimental (measured)
F	frictional
f	saturated liquid
fo	liquid only
g	saturated vapor
pred	predicted
s	solid copper wall
sat	saturated
tp	two-phase
tt	turbulent liquid-turbulent vapor
w	wall; water

While past studies have provided very useful knowhow on condensation in micro-channels, there is a lack of fundamental understanding of interfacial behavior and shortage of predictive tools for both pressure drop and heat transfer coefficient. Two phenomena that are important to modeling condensation in micro-channels are interfacial waves and turbulence in the annular liquid film. The importance of interfacial waves is evident from past studies involving adiabatic, heated and evaporating liquid films [13–18]. Turbulence near the liquid film-vapor interface has been shown to undergo appreciable dampening due to surface tension forces, and this behavior can have a significant influence on heat transfer across the film [19]. These fundamental issues, and the need for reliable correlations for condensing micro-channel flows, are the primary motivation for a series of studies that have recently been initiated at the Purdue University Boiling and Two-Phase Flow Laboratory (BTPFL), including the present study.

The first part of this study [4] examined two-phase flow regimes and pressure drop characteristics of a micro-channel condensation module. The primary objective of this part of the study is to explore the module's condensation heat transfer characteristics. The present FC-72 heat transfer data are first compared with predictions of several previous correlations for both macro-channels [5–9] and mini/micro-channels [10–12]. A new correlation for annular condensation heat transfer is proposed, which is validated against the present data in addition to a database for

condensation in mini/micro-channels from eight previous sources [10,12,20–25].

2. Experimental facility

Fig. 1 shows a schematic of the two-phase facility constructed for the present study. The facility consists of a primary FC-72 cooling loop and a secondary water loop. The FC-72 is condensed along a series of ten 1.0×1.0 mm^2 channels that are formed in the 20-mm wide by 29.9-cm long top surface of a cooper block. The condensation is achieved by rejecting heat to a counter flow of water through three brass channels soldered to the underside of the copper block. The copper block is inserted into an insulating housing made from G-10 fiberglass plastic and fitted atop with a transparent cover plate made from polycarbonate plastic (Lexan). The dimensions of the test section are provided in Table 1.

Using a variac-controlled gear pump, the FC-72 is supplied from the primary loop's reservoir through a flow meter followed by an in-line electric heater before entering the condensation module. A variac is used to regulate electrical power input to the in-line heater and bring the FC-72 to a quality near unity at the inlet to the condensation module. Exiting the condensation module, the FC-72 is fully condensed and brought to the desired temperature
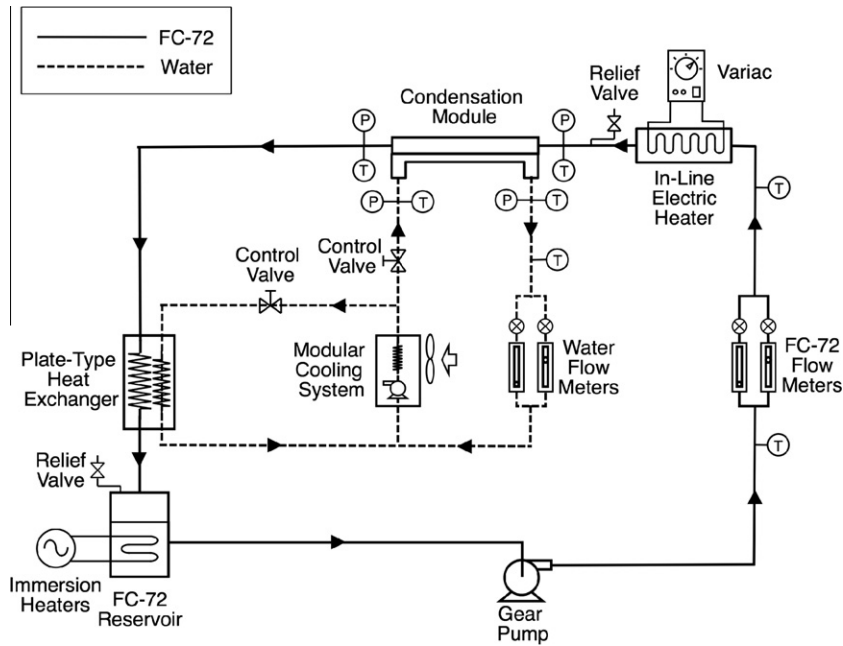
Fig. 1. Schematic diagram of test loop.

Table 1
Test section dimensions.

W_{ch} (mm)	H_{ch} (mm)	W_s (mm)	H_t (mm)	H_b (mm)	L (mm)	N (mm)
1	1	1	9.65	7.62	29.9	10

as it returns to the reservoir by rejecting heat to the secondary water loop via a plate-type heat exchanger.

The water is circulated through the secondary loop using a modular Lytron cooling system. The water flow is divided into two branches. The first routes a portion of the water flow through the condensation module, while the other supplies the remaining flow through the plate-type heat exchanger.

Additional details concerning the test facility, construction of the condensation module, and measurement methods are provided in the first part of this study [4].

3. Heat transfer data reduction

Efforts were made to achieve slightly superheated FC-72 conditions at the inlet to the condensation module. This helped maintain annular flow in the inlet region of the micro-channels and achieve high heat transfer coefficients as well as a broad range of operating conditions.

Fig. 2 shows a unit cell illustrating key parameters that are used in determining the heat transfer performance of the condensation micro-channels. Unlike most boiling experiments, where the heat flux is measured from electrical power input, heat flux in this study is determined from temperature measurements along two parallel planes in the copper block beneath the micro-channels. Sixteen pairs of type-E thermocouples are embedded at 19-mm intervals along the length of the copper block. At each axial thermocouple location, both the heat flux along the base of the micro-channels and the base temperature are determined from temperature measurements by the thermocouple pair using the assumption of one-dimensional heat conduction between the two thermocouple planes.

$$q''_{base} = \frac{k_s(T_t - T_b)}{H_b}. \tag{1}$$

The temperature corresponding to the plane in line with the bottom of the micro-channels can be determined from

$$T_{w,b} = T_t + \frac{q''_{base}H_t}{k_s}. \tag{2}$$

The local rates of sensible heat loss in the superheated vapor region and latent heat loss in the two-phase condensing region from FC-72 can be calculated from the following energy balances, respectively,

$$\frac{\dot{m}}{N}c_{p,g}\Delta T_f = q''_{base}(W_{ch} + W_s)\Delta z, \tag{3a}$$

and

$$\frac{\dot{m}}{N}h_{fg}\Delta x = q''_{base}(W_{ch} + W_s)\Delta z. \tag{3b}$$

It is assumed that the superheated vapor maintains single-phase vapor state until it reaches zero thermodynamic equilibrium quality. The local quality in the superheated region can be determined from

$$x = 1 + \frac{c_{p,g}(T_f - T_{sat})}{h_{fg}}, \tag{4}$$

where the saturation temperature is obtained from the local saturation pressure.

Fig. 3 shows a sample of top and bottom thermocouple temperatures measured along the copper block for three FC-72 mass velocities. The corresponding temperature distribution along the two thermocouple planes is fitted by a third-order or fourth-order polynomial function of axial distance. These distributions are then used to determine the corresponding variations of base heat flux and thermodynamic equilibrium quality. Fig. 3 shows that the base heat flux increases with increasing mass velocity due to the increasing temperature difference between the two thermocouple planes.

Inlet quality was maintained at 1.11–1.17 for low FC-72 mass velocities (G = 68–186 kg/m^{2}s) and 1.08–1.10 for high mass velocities (G = 248–367 kg/m^{2}s), which correspond to a single-phase superheated vapor region 1.1–3.1 cm long (4–10% of the channel
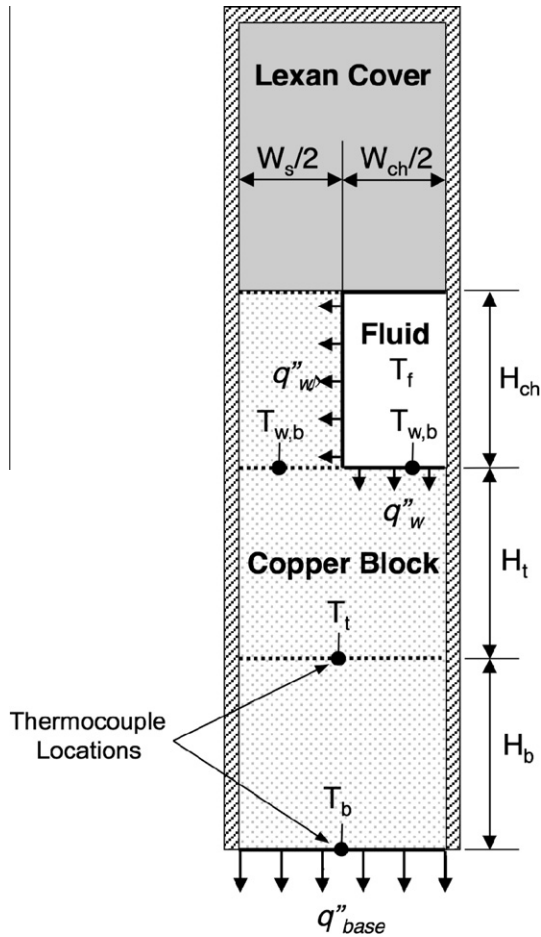
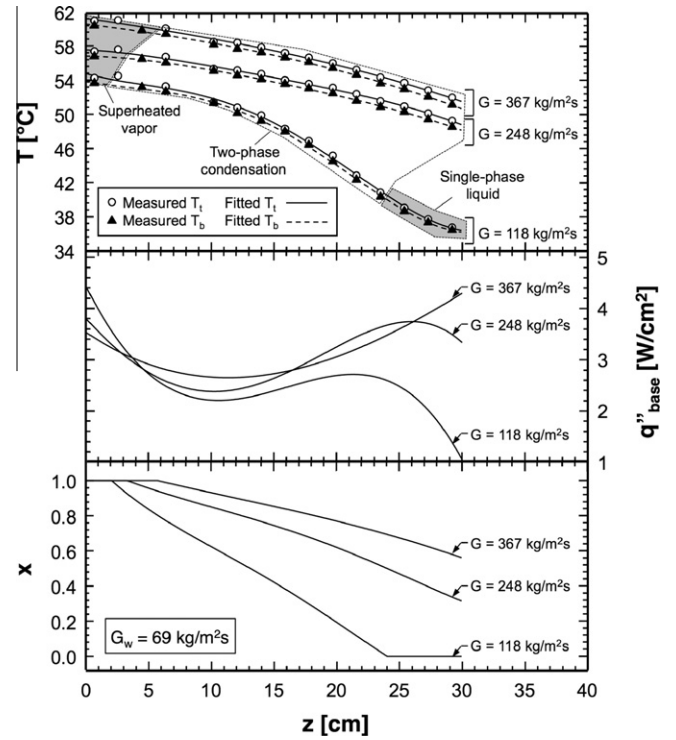Fig. 2. Unit cell for condensation micro-channel.

Fig. 3. Variations of copper block temperatures, base heat flux, and thermodynamic equilibrium quality along stream-wise direction for different FC-72 mass velocities with G_w = 69 kg/m²s.

length) and 2.7–5.8 cm long (9–19% of the channel length), respectively. For the two-phase condensation region ($x \leq 1$), the present study covered the following operating conditions: FC-72 mass velocities of G = 68–367 kg/m²s, FC-72 saturation temperatures of T_{sat} = 57.2–62.3 °C, FC-72 qualities of $x = 1 - 0$, water mass velocities of G_w = 69–138 kg/m²s, and heat fluxes of q''_w = 0.43–3.21 W/cm².

Measurement uncertainties are ±0.5% for the pressure transducer and ±2.0% for the flow meter. Unlike the thermocouples inserted in the flow, the thermocouples embedded in the copper block are carefully calibrated using a procedure that brought down their uncertainties to less than ±0.03 °C. This is achieved by, first, carefully insulating the entire copper block and placing the block in an isothermal enclosure. This procedure is repeated for different enclosure temperatures. Thermocouples are typically off their mean value by ±0.03 °C, and this offset is corrected for the individual copper block thermocouples using a high accuracy HP data acquisition system. By using five thermocouple ports attached to top of the cover plate, heat loss through the cover plate is estimated at less than 2% of the heat input through the base of the micro-channels, which is calculated using the assumption of one-dimensional heat conduction between the two thermocouple planes. For a high mass velocity of G = 367 kg/m²s, the derived average uncertainties of base heat flux, vapor quality, and local heat transfer coefficient are ±4.6%, ±5.1%, and ±7.2%, respectively. For the worst case of a very low mass velocity of G = 68 kg/m²s, the average uncertainties of base heat flux, vapor quality, and local heat transfer coefficient are ±10.7%, ±11.0%, and ±16.1%, respectively.

4. Condensation heat transfer results

4.1. Experimental results

Kim and Mudawar [26,27] showed that the one-dimensional fin analysis method is both convenient and accurate in evaluating the local heat transfer coefficient for micro-channels with rectangular, inverse trapezoidal, triangular, trapezoidal, diamond-shaped, and circular cross sections.

In case of a condenser having rectangular micro-channels with three-sided cooling walls (i.e., assuming a perfectly insulating top cover plate) as illustrated in Fig. 2, applying the fin analysis method yields

$$h = \frac{q''_w(2H_{ch} + W_{ch})}{(T_{w,b} - T_f)(2\eta H_{ch} + W_{ch})} = \frac{q''_{base}(W_s + W_{ch})}{(T_{w,b} - T_f)(2\eta H_{ch} + W_{ch})}, \quad (5)$$

where q''_{base} is the base heat flux, and the fin efficiency and fin parameter are defined, respectively, as [28]

$$\eta = \frac{\tanh(mH_{ch})}{mH_{ch}} \quad (6a)$$

and

$$m = \sqrt{\frac{2h}{k_s W_s}}. \quad (6b)$$

Fig. 4 shows the variation of the experimentally-determined local FC-72 condensation heat transfer coefficient with thermodynamic equilibrium quality in the saturated region for different water mass velocities and FC-72 mass velocities in the range of 68–367 kg/m²s. Very high heat transfer coefficient values are achieved near $x = 1$, where annular flow regime is initiated and the liquid film is very
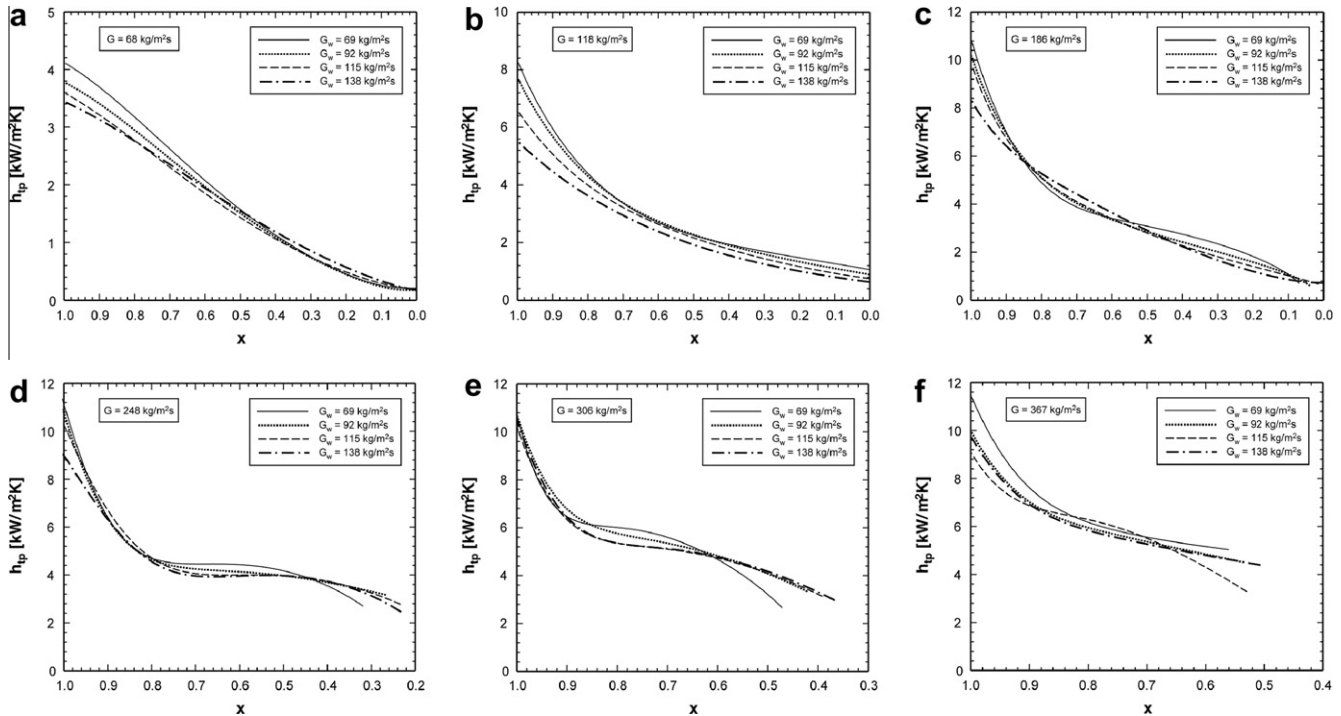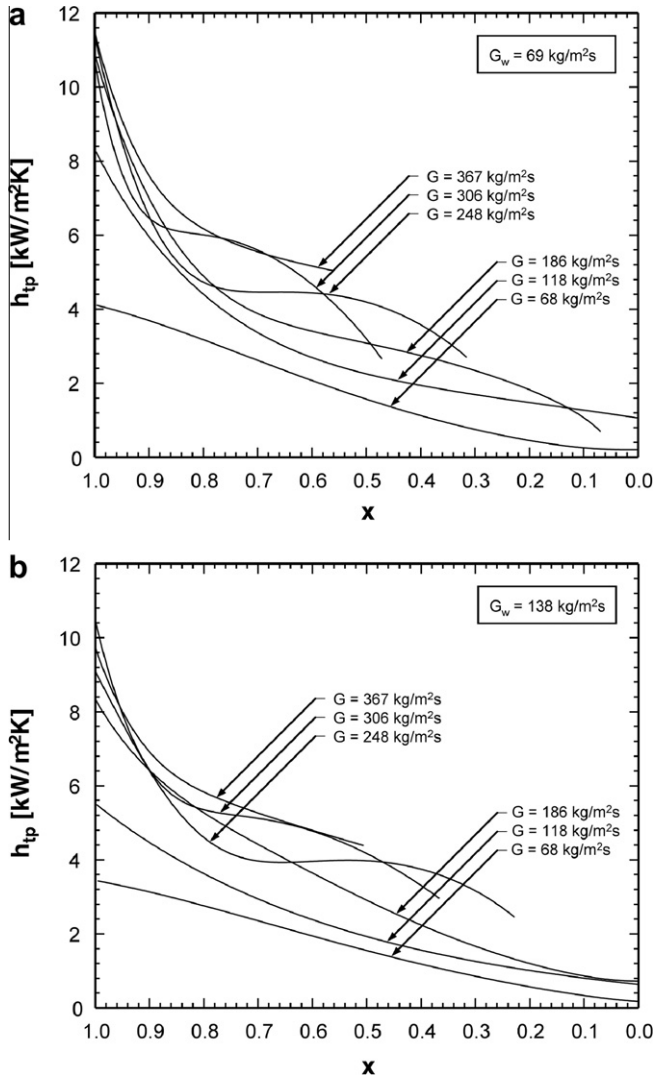
Fig. 4. Variation of experimentally-determined local FC-72 condensation heat transfer coefficient with thermodynamic equilibrium quality for different coolant mass velocities with (a) $G = 68$ kg/m²s, (b) $G = 118$ kg/m²s, (c) $G = 186$ kg/m²s, (d) $G = 248$ kg/m²s, (e) $G = 306$ kg/m²s, and (f) $G = 367$ kg/m²s.

thin. The condensation coefficient decreases along the channel as the film gradually thickens and/or the annular regime is replaced by transition or slug flow regimes. Overall, there is a far stronger sensitivity to FC-72 mass velocity than to water flow rate.

Fig. 5 shows the variation of local FC-72 condensation heat transfer coefficient with thermodynamic equilibrium quality in the saturated region for different FC-72 mass velocities and two water flow rates. Increasing the mass velocity of FC-72 extends the annular regime farther downstream towards lower quality values. Increasing the mass velocity increases the condensation heat transfer coefficient by thinning the liquid film due to the increased interfacial vapor shear stress. Notice that the slope of heat transfer coefficient plot in Fig. 5 decreases appreciably in range of $x = 0.4$–0.7 for $G = 248$ kg/m²s and $x = 0.6$–0.8 for $G = 306$ kg/m²s. As shown in the first part of this study [4], these quality ranges correspond mostly to the wavy-annular regime. It can therefore be inferred that at high mass velocities, interfacial waves enhance the condensation heat transfer by slowing the trend of declining heat transfer coefficient along the channel caused by the film thinning. Notice that the flattening in the variation of h_{tp} versus x is nonexistent for the lower mass velocities. This can be explained by the narrowing of the extent of the wavy annular regime at low mass velocities.

Fig. 6 shows the variation of the average condensation heat transfer coefficient with water mass velocities for different FC-72 mass velocities. It should be emphasized that all of the average condensation heat transfer coefficient data in this figure, as well as Figs. 7, 8 and 12, correspond to values averaged over only the two-phase condensing region (corresponding to the range $x = 0$–1), and exclude the upstream superheated vapor region and downstream single-phase liquid region of the micro-channel. In Fig. 6, the condensation heat transfer coefficient increases with increasing FC-72 mass velocity because of the increased interfacial shear stress and resulting liquid film thinning. On the other hand, increasing the water flow rate increases the flow rate of FC-72 and film thickness, casing a reduction in the heat transfer coefficient.

4.2. Comparison with previous heat transfer correlations

Table 2 provides a summary of select condensation heat transfer correlations for the annular flow regime. The predictive accuracy of the correlations is measured by mean absolute error, which is defined as

$$MAE = \frac{1}{M} \sum \frac{|\bar{h}_{tp,pred} - \bar{h}_{tp,exp}|}{\bar{h}_{tp,exp}} \times 100\%. \tag{7}$$

The correlations in Table 2 can be classified into the following categories: two-phase multiplier-based correlations (Akers et al. [5], Shah [7], Dobson and Chato [9]), and boundary layer-based correlations (Cavallini and Zecchin [6], Moser et al. [8], Wang et al. [10], Koyama et al. [11], Huang et al. [12]). Notice that the correlations of Koyama et al. and Huang et al. are based on Haraguchi et al.'s [29] boundary layer-based correlation. Since the correlations in Table 2 are intended for uniform circumferential cooling in circular tubes or rectangular channels with four-sided cooling, a multiplier must be adopted when applying these correlations to condensation in rectangular micro-channels with three-sided wall cooling (i.e., with a perfectly insulating top cover plate). Following a technique adopted by Qu and Mudawar [30] and Lee and Mudawar [31] to correct for three-sided heating in flow boiling, the condensation heat transfer coefficient for three-sided cooling is related to that obtained from a correlation for uniform circumferential cooling by the relation

$$h_{tp} = \left(\frac{Nu_3}{Nu_4}\right) h_{tp,cir}, \tag{8}$$

where $h_{tp,cir}$ is the heat transfer correlation based on uniform circumferential cooling, and Nu_3 and Nu_4 are Nusselt numbers for thermally developed laminar flow with three-sided and four-sided heat transfer, respectively, [32]

$$Nu_3 = 8.235(1 - 1.833\beta + 3.767\beta^2 - 5.814\beta^3 + 5.361\beta^4 - 2.0\beta^5) \tag{9a}$$

and

$$Nu_4 = 8.235(1 - 2.042\beta + 3.085\beta^2 - 2.477\beta^3 + 1.058\beta^4 - 0.186\beta^5).$$

(9b)

Fig. 7(a) compares the present FC-72 average condensation heat transfer coefficient data, which correspond mostly to the smooth-annular, wavy-annular, and transition flow regimes, to predictions of five correlations for annular flow condensation in macro-channels. Four of the correlations show good to fair predictions of the present data, while the correlation by Akers et al. [5] highly over-predicts the present data. Notably, the correlations of Cavallini and Zecchin [6], Shah [7], and Dobson and Chato [9] predict the present FC-72 data with MAEs of 8.42%, 13.32%, and 10.65%, respectively.

Fig. 7(b) compares the present FC-72 average condensation heat transfer coefficient data with predictions of annular condensation heat transfer correlations intended for mini/micro-channels. Wang et al. [10] developed a boundary layer-based correlation for annular flow in which the two-phase frictional multiplier and dimensionless boundary layer temperature were evaluated for R134a condensing inside a horizontal rectangular multi-channel with a hydraulic diameter of 1.46 mm. The correlation of Koyama et al. [11] is based on Haraguchi et al.'s [29] correlation for annular flow, which is derived from boundary layer analysis for condensation of R22, R134a, and R123 inside a horizontal 8.4 mm diameter circular tube and Mishima and Hibiki's [33] correlation for the two-phase frictional multiplier. Huang et al.'s [12] correlation is based on Haraguchi et al.'s [34] frictional multiplier correlation for a diameter of 8.4 mm and Haraguchi et al.'s [29] annular condensation correlation, which Huang et al. modified with their own experimental data. Although the correlations in Fig. 7(b) are intended for mini/micro-channels, they show relatively poor agreement with the present FC-72 data compared to the top four macro-channel correlations in Fig. 7(a).

4.3. New heat transfer correlation

For a shear-dominated annular condensing flow, the local condensation heat transfer coefficient of liquid film can be obtained from the following relation,

$$h_{tp,cir} = \frac{q''_w}{T_{sat} - T_w} = \frac{\rho_f c_{p,f} u^*}{T_\delta^+},$$

(10)

where the friction velocity and dimensionless boundary layer temperature are defined, respectively, as

$$u^* = \sqrt{\tau_w / \rho_f},$$

(11a)

and

$$T_\delta^+ = \int_0^{\delta^+} \frac{q''}{q''_w} \left(\frac{1}{Pr_f} + \frac{1}{Pr_T} \frac{\varepsilon_m}{v_f} \right)^{-1} dy^+.$$

(11b)

The wall shear stress can be expressed as a function of the single-phase frictional pressure drop based on liquid flow and the two-phase frictional multiplier,

$$\tau_w = -\left(\frac{dP}{dz} \right)_F \frac{D_h}{4} = -\left(\frac{dP}{dz} \right)_f \frac{D_h}{4} \phi_f^2.$$

(12)

The single-phase frictional pressure drop based on liquid flow can be expressed as

$$-\left(\frac{dP}{dz} \right)_f = \frac{2fG^2(1-x)^2 v_f}{D_h}.$$

(13)

Fig. 5. Variation of experimentally-determined local FC-72 condensation heat transfer coefficient with thermodynamic equilibrium quality for different FC-72 mass velocities with (a) G_w = 69 kg/m²s, and (b) G_w = 138 kg/m²s.
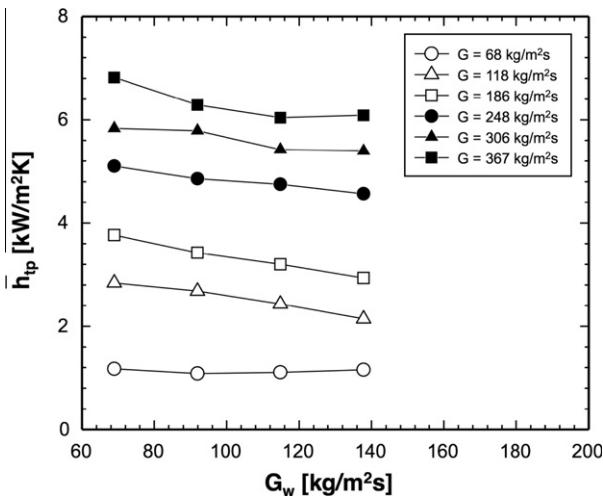

Fig. 6. Variation of experimentally-determined average FC-72 condensation heat transfer coefficient with coolant mass velocity for different FC-72 mass velocities.
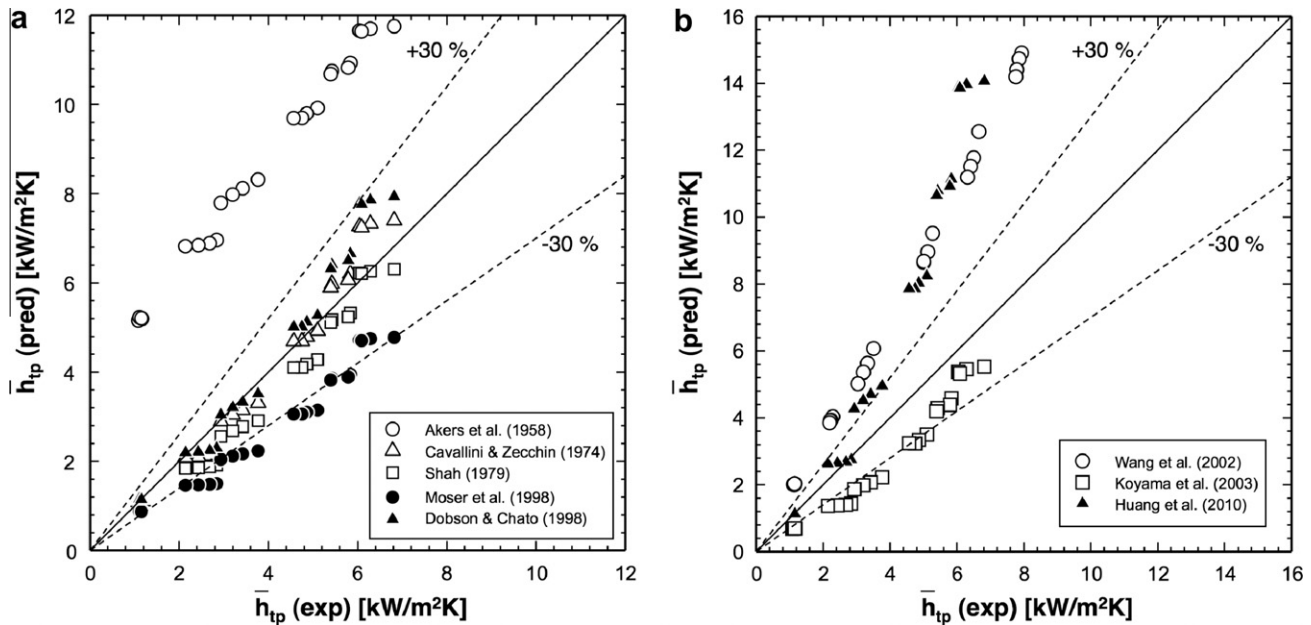
Fig. 7. Comparison of present experimentally-determined average FC-72 condensation heat transfer coefficient data with predictions of (a) annular flow macro-channel condensation correlations, and (b) annular flow mini/micro-channel condensation correlations.
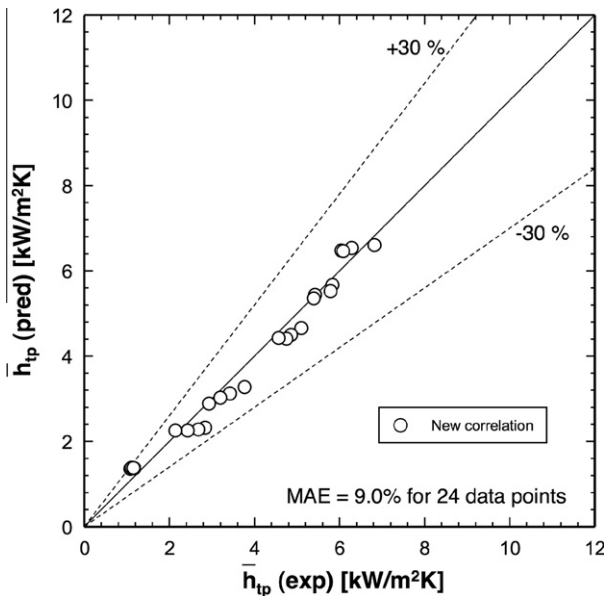

Fig. 8. Comparison of present experimentally-determined average FC-72 condensation heat transfer coefficient data with predictions of the new annular condensation correlation.

The correlation of Mishima and Hibiki [33], which is based on adiabatic air–water two-phase flow inside 1–4 mm diameter circular tubes, showed good predictions of experimental pressure drop data in small channels such as circular tubes (Cavallini et al. [23]), trapezoidal channels (Quan et al. [35]), and rectangular channels (Koyama et al. [11], Park and Hrnjak [24], Qu and Mudawar [36]). Mishima and Hibiki's correlation also provided the best predictions of the present FC-72 pressure drop data (MAE of 27.15%) among all the separated flow correlations examined in part 1 of the study [4]. Therefore, the two-phase frictional multiplier in Eq. (12) is based on Mishima and Hibiki's correlation

$$\phi_f^2 = 1 + \frac{21[1 - \exp(-0.319D_h)]}{X} + \frac{1}{X^2}, \quad D_h[mm]. \tag{14}$$

It was shown earlier that most macro-channel correlations intended for circular tubes provide good agreement with the present square micro-channel condensation heat transfer data. This suggests that, unlike non-annular flow regimes, there are no major differences in condensation behavior between small and large channels in the annular regime. Furthermore, the low surface tension of FC-72 tends to maintain nearly uniform liquid film thickness along the inner walls of the square channel, barely affected by corner effects. Therefore, the following relation by Haraguchi et al. [29] for condensation of R22, R134a, and R123 inside an 8.4-mm horizontal circular tube with $G = 200$–400 kg/m²s is used for determination of the dimensionless boundary layer temperature in the present square micro-channel,

$$T_\delta^+ = (0.1 + 0.06Pr_f^{0.8})^{-1}Pr_f Re_f^{0.13}. \tag{15}$$

Substituting Eqs. (11)–(15) into Eq. (10), and accounting for the effects of three-sided cooling via Eq. (8), the local heat transfer coefficient for annular condensation with three-sided cooling can be expressed as

$$h_{tp} = \left(\frac{Nu_3}{Nu_4}\right)\left(0.1 + 0.06Pr_f^{0.8}\right)Pr_f^{-1}Re_f^{-0.13}c_{p,f}$$

$$\times \sqrt{\frac{fG^2(1-x)^2}{2}\left\{1 + \frac{21[1 - \exp(-0.319D_h)]}{X} + \frac{1}{X^2}\right\}}, \tag{16}$$

where X is the Martinelli parameter. The Fanning friction factor based on liquid flow can be determined from [28,32].

$$fRe_f = 24(1 - 1.3553\beta + 1.9467\beta^2 - 1.7012\beta^3$$
$$+ 0.9564\beta^4 - 0.2537\beta^5) \quad \text{for } Re_f < 2000, \tag{17a}$$

$$f = 0.079Re_f^{-0.25} \text{ for } 2000 \leq Re_f < 20,000, \tag{17b}$$

$$f = 0.046Re_f^{-0.2} \text{ for } Re_f \geq 20,000, \quad \text{and } Re_f = G(1-x)D_h/\mu_f. \tag{17c}$$

Fig. 8 shows the new condensation heat transfer correlation accurately predicts the present FC-72 average heat transfer data with
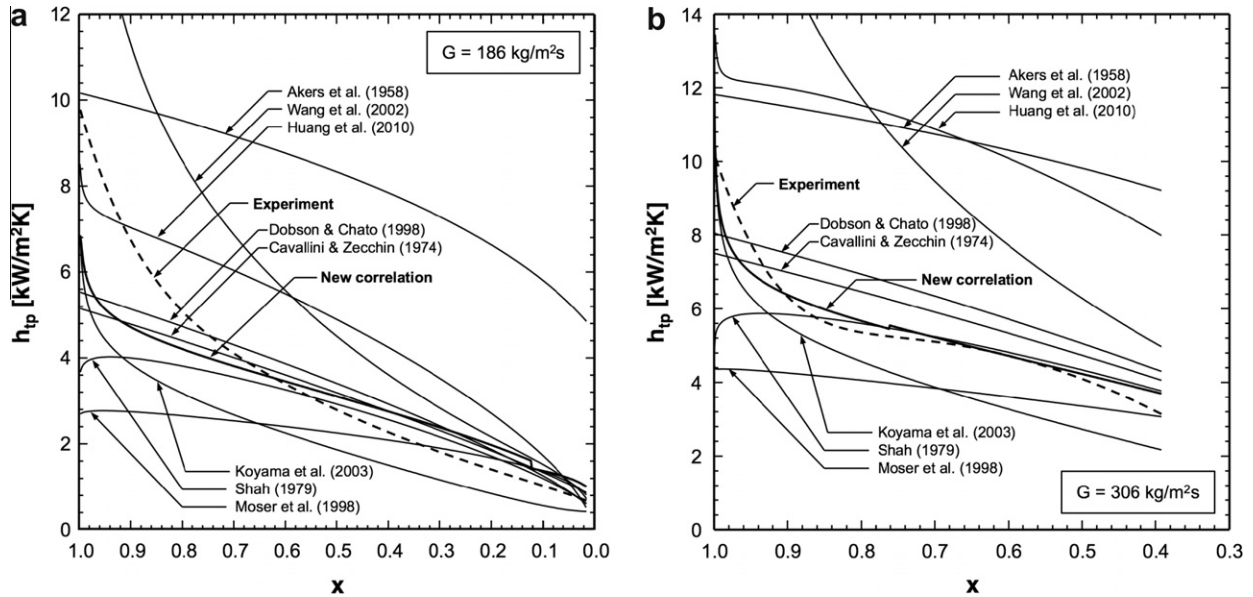
Fig. 9. Variation of present experimentally-determined local FC-72 condensation heat transfer coefficient data with thermodynamic equilibrium quality compared to predictions of new correlation and previous annular condensation correlations for G_w = 115 kg/m²s with (a) G = 186 kg/m²s, and (b) G = 306 kg/m²s.

Table 2
Condensation heat transfer correlations for annular flow regime with corresponding MAE in predicting present experimental data.

Author(s)	Equation	Remarks	MAE [%]
Akers et al. [5]	$\frac{h_{tp}D_h}{k_f} = \left(\frac{Nu_3}{Nu_4}\right)0.0265\mathrm{Re}_{eq}^{0.8}Pr_f^{1/3}$ for $\mathrm{Re}_{eq} > 50000$ $\frac{h_{tp}D_h}{k_f} = \left(\frac{Nu_3}{Nu_4}\right)5.03\mathrm{Re}_{eq}^{1/3}Pr_f^{1/3}$ for $\mathrm{Re}_{eq} \le 50000$ $\mathrm{Re}_{eq} = G\left[(1-x) + x\left(\frac{\rho_f}{\rho_g}\right)^{0.5}\right]\frac{D_h}{\mu_f}$	Fluids: R12, propane All flow regimes $60 \le NuPr_f^{-1/3} \le 400$	160
Cavallini and Zecchin [6]	$\frac{h_{tp}D}{k_f} = \left(\frac{Nu_3}{Nu_4}\right)0.05\mathrm{Re}_f^{0.8}Pr_f^{0.33}\left[1 + \left(\frac{\rho_f}{\rho_g}\right)^{0.5}\left(\frac{x}{1-x}\right)\right]^{0.8}$	Fluids: R12, R22, R113 $7000 \le \mathrm{Re}_{fo} \le 53000$	8.42
Shah [7]	$\frac{h_{tp}D_h}{k_f} = \left(\frac{Nu_3}{Nu_4}\right)0.023\mathrm{Re}_{fo}^{0.8}Pr_f^{0.4}\left[(1-x)^{0.8} + \frac{3.8x^{0.76}(1-x)^{0.04}}{P_R^{0.38}}\right]$	D = 7–40 mm Fluids: water, R11, R12, R22, R113, methanol, ethanol, benzene, toluene, trichloroethylene	13.32
Moser et al. [8]	$\frac{h_{tp}D_h}{k_f} = \left(\frac{Nu_3}{Nu_4}\right)\frac{0.0994^{C_1}\mathrm{Re}_f^{C_2}\mathrm{Re}_{eq}^{1+0.875C_1}Pr_f^{0.815}}{(1.58\ln\mathrm{Re}_{eq}-3.28)(2.58\ln\mathrm{Re}_{eq}+13.7Pr_f^{2/3}-19.1)}$ $C_1 = 0.126Pr_f^{-0.448}, C_2 = -0.113Pr_f^{-0.563}, \mathrm{Re}_{eq} = \phi_{fo,Friedel}^{8/7}\mathrm{Re}_{fo}$	D = 3.14–20 mm Fluids: R11, R12, R125, R22, R134a, R410A 1197 data points	31.79
Dobson and Chato [9]	$\frac{h_{tp}D_h}{k_f} = \left(\frac{Nu_3}{Nu_4}\right)0.023\mathrm{Re}_f^{0.8}Pr_f^{0.4}\left(1 + \frac{2.22}{X_{tt}^{0.89}}\right)$ $X_{tt} = \left(\frac{\mu_f}{\mu_g}\right)^{0.1}\left(\frac{1-x}{x}\right)^{0.9}\left(\frac{v_f}{v_g}\right)^{0.5}$	D = 3.14–7.04 mm Fluids: R12, R22, R134a, R32/R125	10.65
Wang et al. [10]	$\frac{h_{tp}D_h}{k_f} = \left(\frac{Nu_3}{Nu_4}\right)0.0274Pr_f\mathrm{Re}_f^{0.6792}x^{0.2208}\frac{\phi_g}{X_{tt}}$ $\phi_g^2 = 1.376 + 8X_{tt}^{1.665}$	D_h = 1.46 mm Fluid: R134a Multi-channel	88.03
Koyama et al. [11]	$\frac{h_{tp}D_h}{k_f} = \left(\frac{Nu_3}{Nu_4}\right)0.0152(1 + 0.6Pr_f^{0.8})\frac{\phi_g}{X_{tt}}\mathrm{Re}_f^{0.77}$ $\phi_g^2 = 1 + 21[1 - \exp(-0.319D_h)]X_{tt} + X_{tt}^2$	D_h = 0.80, 1.11 mm Fluid: R134a Multi-channel	31.35
Huang et al. [12]	$\frac{h_{tp}D}{k_f} = \left(\frac{Nu_3}{Nu_4}\right)0.0152(-0.33 + 0.83Pr_f^{0.8})\frac{\phi_g}{X_{tt}}\mathrm{Re}_f^{0.77}$ $\phi_g^2 = 1 + 0.5\left\{\frac{G}{[gD_h\rho_g(\rho_f-\rho_g)]^{0.5}}\right\}^{0.75}X_{tt}^{0.35}$	D = 1.6, 4.18 mm Fluids: R410A, R410A/oil	55.31

a mean absolute error of 9.0%, although some low mass velocity data include non-annular data.

Fig. 9 compares the present local heat transfer coefficient data for G = 186 and 306 kg/m²s and G_w = 115 kg/m²s with predictions of the new correlation, Eq. (16), and previous correlations given in Table 2. The new correlation shows best predictions of the present data both in magnitude and trend. The correlations of Akers et al. [5], Wang et al. [10] and Huang et al. [12] over-predict the data by an appreciable margin. While the Shah [7] correlation predicts an unrealistic trend of decreasing heat transfer coefficient in the

high vapor quality region where the film is thinnest, this correlation provides good overall prediction of the average heat transfer coefficient, evidenced by a MAE of 13.32%.

In order to further assess the accuracy of the new annular condensation heat transfer correlation, a total 923 data points for condensation in mini/micro-channels were amassed from eight sources which are described in Table 3. Fig. 10 shows all 923 data points in a plot of Martinelli parameter based on turbulent liquid-turbulent vapor versus modified Weber number, which is defined by Soliman [37] as

Table 3
Database for two-phase condensation heat transfer coefficient in mini/micro-channels.

Author(s)	D_h [mm]	Fluid (s)	Geometry[*]	All data/annular data[+]
Hirofumi and Webb [20]	0.96–2.13	R134a	C/R multi	62/61
Zhang [21]	2.13, 3.25	R134a, R22, R404A	C single/multi	66/65
Yan and Lin [22]	2.0	R134a	C multi	78/60
Wang et al. [10]	1.46	R134a	R multi	410/268
Cavallini et al. [23]	1.4	R134a, R410A	R multi	59/56
Park and Hrnjak [24]	0.89	CO_2	C multi	52/37
Matkovic et al. [25]	0.96	R134a, R32	C single	161/131
Huang et al. [12]	1.6, 4.18	R410A	C single	35/35

[*] C: circular, R: rectangular, [+]annular data (smooth-annular, wavy-annular and transition) correspond to $We^* > 7X_{tt}^{0.2}$.
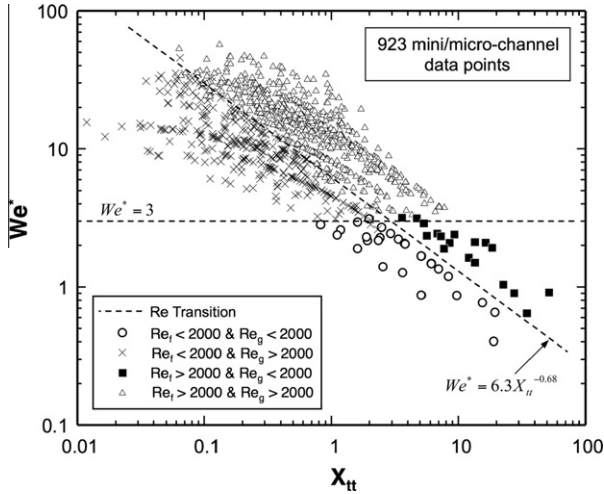
Fig. 10. Reynolds number transition lines based on 923 mini/micro-channel data points from eight sources.

$$We^* = 2.45 \frac{Re_g^{0.64}}{Su_g^{0.3}(1 + 1.09X_{tt}^{0.039})^{0.4}} \quad \text{for } Re_f \leq 1250, \tag{18a}$$

and

$$We^* = 0.85 \frac{Re_g^{0.79}X_{tt}^{0.157}}{Su_g^{0.3}(1 + 1.09X_{tt}^{0.039})^{0.4}} \left[\left(\frac{\mu_g}{\mu_f} \right)^2 \left(\frac{\upsilon_g}{\upsilon_f} \right) \right]^{0.084}$$

for $Re_f > 1250$, (18b)

where the Suratman number, Su_g, and the turbulent-turbulent Martinelli parameter, X_{tt}, are defined as

$$Su_g = \frac{\rho_g \sigma D}{\mu_g^2} \tag{19a}$$

and

$$X_{tt} = \left(\frac{\mu_f}{\mu_g} \right)^{0.1} \left(\frac{1-x}{x} \right)^{0.9} \left(\frac{\upsilon_f}{\upsilon_g} \right)^{0.5}, \tag{19b}$$

respectively [37]. The vapor and liquid Reynolds numbers of the 923 data points are also symbolized in Fig. 10 with a transition Reynolds number value of 2000. Although all the data are plotted versus the turbulent-turbulent Martinelli parameter, they are classified clearly into the following four different zones by two fitted lines of $We^* = 3$ and $We^* = 6.3X_{tt}^{-0.68}$,

$Re_f < 2000$ and $Re_g < 2000$: $We^* < 3$ and $We^* < 6.3X_{tt}^{-0.68}$.
(20a)

$Re_f < 2000$ and $Re_g > 2000$: $3 < We^* < 6.3X_{tt}^{-0.68}$. (20b)

$Re_f > 2000$ and $Re_g < 2000$: $6.3X_{tt}^{-0.68} < We^* < 3$. (20c)

$Re_f > 2000$ and $Re_g > 2000$: $We^* > 3$ and $We^* > 6.3X_{tt}^{-0.68}$.
(20d)

Based on the FC-72 flow visualization data presented in the first part of this study [4], the following lines are fitted for boundaries between different flow regimes:

Smooth – annular to wavy – annular : $We^* = 90X_{tt}^{0.5}$. (21a)

Wavy – annular to transition : $We^* = 24X_{tt}^{0.41}$. (21b)

Transition to slug : $We^* = 7X_{tt}^{0.2}$. (21c)

Cavallini et al. [38] proposed that the flow is annular for $J_g^* > 2.5$, and intermittent and slug for $J_g^* < 2.5$, based on previous flow regime maps, where the dimensionless superficial vapor velocity is defined as

$$J_g^* = Gx / \sqrt{\rho_g(\rho_g - \rho_g)gD}. \tag{22}$$

Fig. 11 shows 639 mini/micro-channel annular data points from the eight aforementioned sources excluding all data with dimensionless superficial gas velocities below 2.5. Although a few data points do appear for $We^* < 7X_{tt}^{0.2}$, the boundary line between the transition and slug regimes from the present study is in general agreement with that from Cavallini et al.
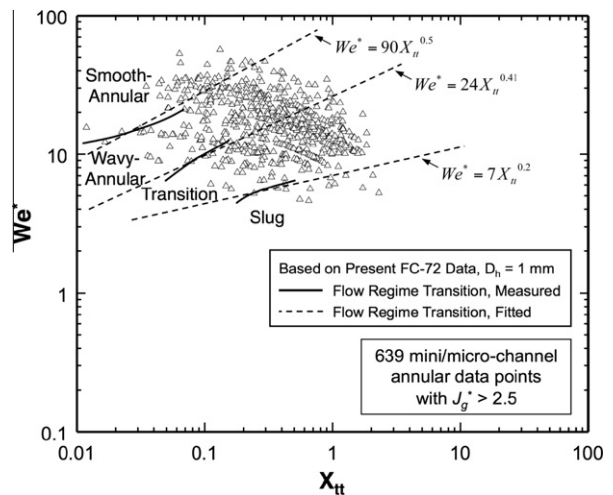

Fig. 11. Proposed flow regime map based on present FC-72 flow visualization experiments in square micro-channels with $D_h = 1$ mm plotted alongside 639 mini/micro-channel data points corresponding to $J_g^* > 2.5$ from eight sources.

Table 4
Comparison of mini/micro-channel database for annular flow (smooth-annular, wavy-annular and transition) with predictions of annular condensation heat transfer correlations.

Author(s)	Mean absolute error [%]								
	Akers et al. [5]	Cavallini and Zecchin [6]	Shah [7]	Moser et al. [8]	Dobson and Chato [9]	Wang et al. [10]	Koyama et al. [11]	Huang et al. [12]	New correl.
Hirofumi and Webb [20]	89.1	84.9	72.4	39.1	77.9	12.3	30.2	93.3	29.3
Zhang [21]	27.6	32.6	22.5	10.6	27.8	33.7	50.4	25.8	15.5
Yan and Lin [22]	84.5	16.8	12.0	11.8	16.4	21.0	48.3	34.0	13.4
Wang et al. [10]	27.2	59.8	45.8	22.2	46.5	14.1	45.5	28.7	16.8
Cavallini et al. [23]	53.3	33.5	23.7	12.6	28.7	33.6	49.9	34.3	17.1
Park and Hrnjak [24]	178.3	73.6	54.6	40.8	67.7	14.7	30.0	53.8	11.0
Matkovic et al. [25]	59.6	29.9	18.8	14.0	26.8	34.5	48.4	52.3	21.6
Huang et al. [12]	12.8	19.1	15.2	15.8	17.4	48.2	57.3	39.9	20.8
Total	90.1	47.0	35.4	20.1	39.6	23.3	45.5	39.4	18.3
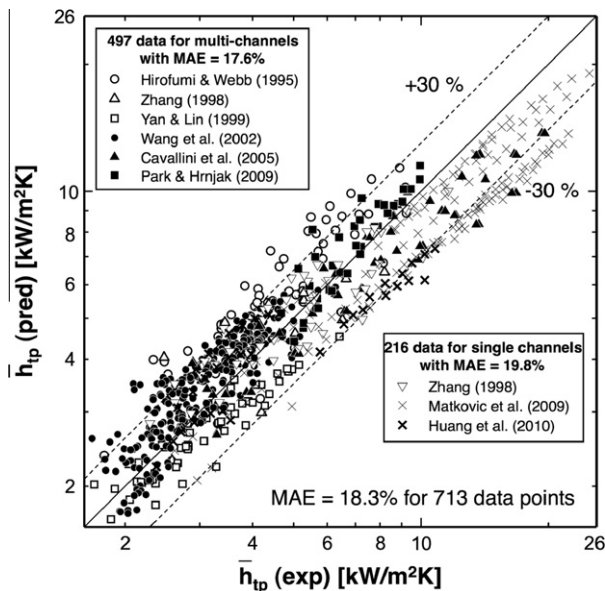
Fig. 12. Comparison of predictions of new annular condensation heat transfer correlation with prior experimental mini/micro-channel data.

In order to isolate data corresponding to flow regimes with a clearly identifiable annular liquid film (smooth-annular, wavy-annular and transition) to assess the accuracy of the new correlation, all 210 data points (from a total of 923 data pints) that correspond to $We^* < 7X_{tt}^{0.2}$ are excluded. Table 3 shows both the total number of data points from each of the eight previous sources as well as corresponding number of data points that are deemed to fall into the present broad classification of annular flows.

Table 4 compares the predictive accuracy of previous correlations and the new annular flow correlation against the mini/micro-channel data that fall into the broad classification of annular flows. Although the correlations of Moser et al. [8] and Wang et al. [10] provide good predictive capability against the entire annular database, with MAEs of 20.1% and 23.3%, respectively, they are far less accurate in predicting the present FC-72 data, with corresponding MAEs of 31.8% and 88.0%, respectively. The new annular heat transfer correlation accurately predicts each of the eight previous sources with a MAE less than 30%.

Fig. 12 shows the new annular correlation provides the best prediction of 713 annular mini/micro-channels data points with an overall MAE of 18.3% (17.6% for multi-channels and 19.8% for single channels). Most data points are shown falling within ±30% of predicted values.

5. Conclusions

This study concerns transport phenomena associated with condensation in micro-channels. The first part of this study examined experimental methods that were used to investigate two-phase flow regimes, pressure drop, and heat transfer associated with condensation of FC-72 along parallel square micro-channels with D_h = 1 mm. Also included in the first part was an assessment of the accuracy of prior models and correlations in predicting the present pressure drop data. This part of this study examined the heat transfer characteristics of the condensation test module. FC-72 condensation heat transfer coefficient data were compared to predictions of previous correlations, and a new correlation was developed for the annular regime. The accuracy of this correlation was ascertained against both the present FC-72 data and a large mini/micro-channel database from eight previous sources. Key findings from this study are as follows:

(1) The FC-72 condensation heat transfer coefficient is highest at the point of commencement of the smooth-annular regime, where the annual liquid film is thinnest. The heat transfer coefficient decreases along the micro-channel because of gradual thickening of the liquid film and eventual collapse of the annular regime. For high mass velocities, the variation of the heat transfer coefficient is flatter for intermediate quality values corresponding to the wavy-annular regime, where heat transfer enhancement by the interfacial waves partially compensates for the film thinning.

(2) The FC-72 condensation heat transfer coefficient decreases with increasing water flow rate because of the increased rate of condensation and resulting thickening of the annular liquid film. However, the condensation heat transfer coefficient is less sensitive to variations in coolant mass flow rate than in FC-72 mass velocity.

(3) In general, prior annular condensation heat transfer correlations intended for macro-channels provide better predictions of the present average FC-72 condensation heat transfer coefficient than more recent correlations intended specifically for mini/micro-channels.

(4) A new condensation heat transfer coefficient correlation is proposed for annular condensation heat transfer in mini/micro-channels. This correlation accurately predicts the present FC-72 average heat transfer data with a MAE of 9.0%.

(5) To further assess the predictive accuracy of the new correlation, a database of 923 data points for mini/micro-channels (including multi-channels and single channels) was amassed from eight previous sources, of which 713 data points correspond to annular flow. The new correlation shows excellent predictive capability based on the 713 annular data, evidenced by an overall MAE of 18.3%.

Acknowledgement

References

[1] J. Lee, I. Mudawar, Fluid flow and heat transfer characteristics of low temperature two-phase micro-channel heat sinks – part 1: experimental methods and flow visualization results, Int. J. Heat Mass Transfer 51 (2008) 4315–4326.

[2] J. Lee, I. Mudawar, Fluid flow and heat transfer characteristics of low temperature two-phase micro-channel heat sinks – part 2: subcooled boiling pressure drop and heat transfer, Int. J. Heat Mass Transfer 51 (2008) 4327–4341.

[3] I. Mudawar, D.C. Wadsworth, Critical heat flux from a simulated electronic chip to a confined rectangular impinging jet of dielectric liquid, Int. J. Heat Mass Transfer 34 (1991) 1465–1480.

[4] S.M. Kim, J. Kim, I. Mudawar, Flow condensation in parallel micro-channels – part 1: experimental results and assessment of pressure drop correlations, Int. J. Heat Mass Transfer 55 (2012) 971–983.

[5] W.W. Akers, H.A. Deans, O.K. Crosser, Condensing heat transfer within horizontal tubes, Chem. Eng. Prog. 54 (1958) 89–90.

[6] A. Cavallini, R. Zecchin, A dimensionless correlation for heat transfer in forced convection condensation, in: Proc. 5th Int. Heat Transfer Conf. 3 (1974) pp. 309–313, Tyoko, Japan.

[7] M.M. Shah, A general correlation for heat transfer during film condensation inside pipes, Int. J. Heat Mass Transfer 22 (1979) 547–556.

[8] K.W. Moser, R.L. Webb, B. Na, A new equivalent Reynolds number model for condensation in smooth tubes, ASME J. Heat Transfer 120 (1998) 410–417.

[9] M.K. Dobson, J.C. Chato, Condensation in smooth horizontal tubes, ASME J. Heat Transfer 120 (1998) 193–213.

[10] W.-W. Wang, T.D. Radcliff, R.N. Christensen, A condensation heat transfer correlation for millimeter-scale tubing with flow regime transition, Exp. Therm. Fluid Sci. 26 (2002) 473–485.

[11] S. Koyama, K. Kuwahara, K. Nakashita, K. Yamamoto, An experimental study on condensation of refrigerant R134a in a multi-port extruded tube, Int. J. Refrigerat. 24 (2003) 425–432.

[12] X. Huang, G. Ding, H. Hu, Y. Zhu, H. Peng, Y. Gao, B. Deng, Influence of oil on flow condensation heat transfer of R410A inside 4.18 mm and 1.6 mm inner diameter horizontal smooth tubes, Int. J. Refrigerat. 33 (2010) 158–169.

[13] J.A. Shmerler, I. Mudawar, Local heat transfer coefficient in wavy free-falling turbulent liquid films undergoing uniform sensible heating, Int. J. Heat Mass Transfer 31 (1988) 67–77.

[14] J.A. Shmerler, I. Mudawar, Local evaporative heat transfer coefficient in turbulent free-falling liquid films, Int. J. Heat Mass Transfer 31 (1988) 731–742.

[15] T.H. Lyu, I. Mudawar, Statistical investigation of the relationship between interfacial waviness and sensible heat transfer to a falling liquid film, Int. J. Heat Mass Transfer 34 (1991) 1451–1464.

[16] T.H. Lyu, I. Mudawar, Determination of wave-induced fluctuations of wall temperature and convective heat transfer coefficient in the heating of a turbulent falling liquid film, Int. J. Heat Mass Transfer 34 (1991) 2521–2534.

[17] I. Mudawar, R.A. Houpt, Mass and momentum transport in falling liquid films laminarized at relatively high Reynolds numbers, Int. J. Heat Mass Transfer 36 (1993) 3437–3448.

[18] I. Mudawar, R.A. Houpt, Measurement of mass and momentum transport in wavy-laminar falling liquid films, Int. J. Heat Mass Transfer 36 (1993) 4151–4162.

[19] I. Mudawar, M.A. El-Masri, Momentum and heat transfer across freely-falling turbulent liquid films, Int. J. Multiphase Flow 12 (1986) 771–790.

[20] H. Hirofumi, R.L. Webb, Condensation in extruded aluminum tubes, Penn State Research Report, Showa Aluminum Corporation, 1995.

[21] M. Zhang, A new equivalent Reynolds number model for vapor shear-controlled condensation inside smooth and micro-fin tubes, PhD Thesis, The Pennsylvania State University, PA, 1998.

[22] Y.-Y. Yan, T.-F. Lin, Condensation heat transfer and pressure drop of refrigerant R-134a in a small pipe, Int. J. Heat Mass Transfer 42 (1999) 697–708.

[23] A. Cavallini, D.D. Col, L. Doretti, M. Matkovic, L. Rossetto, C. Zilio, Condensation heat transfer and pressure gradient inside multiport minichannels, Heat Transfer Eng. 26 (2005) 45–55.

[24] C.Y. Park, P. Hrnjak, CO_2 flow condensation heat transfer and pressure drop in multi-port microchannels at low temperatures, Int. J. Refrigeration 32 (2009) 1129–1139.

[25] M. Matkovic, A. Cavallini, D.D. Col, L. Rossetto, Experimental study on condensation heat transfer inside a single circular minichannel, Int. J. Heat Mass Transfer 52 (2009) 2311–2323.

[26] S.M. Kim, I. Mudawar, Analytical heat diffusion models for different micro-channel heat sink cross-sectional geometries, Int. J. Heat Mass Transfer 53 (2010) 4002–4016.

[27] S.M. Kim, I. Mudawar, Analytical heat diffusion models for heat sinks with circular micro-channels, Int. J. Heat Mass Transfer 53 (2010) 4552–4566.

[28] F.P. Incropera, D.P. Dewitt, Fundamentals of Heat and Mass Transfer, 5th ed., Wiley, New York, 2002.

[29] H. Haraguchi, S. Koyama, T. Fujii, Condensation of refrigerants HCFC 22, HFC 134a and HCFC 123 in a horizontal smooth tube (2nd report), Trans. JSME (B) 60 (1994) 245–252.

[30] W. Qu, I. Mudawar, Flow boiling heat transfer in two-phase micro-channel heat sinks-I. Experimental investigation and assessment of correlation methods, Int. J. Heat Mass Transfer 46 (2003) 2755–2771.

[31] J. Lee, I. Mudawar, Two-phase flow in high-heat-flux micro-channel heat sink for refrigeration cooling applications: part II – heat transfer characteristics, Int. J. Heat Mass Transfer 48 (2005) 941–955.

[32] R.K. Shah, A.L. London, Laminar Flow Forced Convection in Ducts: A Source Book for Compact Heat Exchanger Analytical Data, Academic press, New York, 1978. Supl 1.

[33] K. Mishima, T. Hibiki, Some characteristics of air–water two-phase flow in small diameter vertical tubes, Int. J. Multiphase Flow 22 (1996) 703–712.

[34] H. Haraguchi, S. Koyama, T. Fujii, Condensation of refrigerants HCFC 22, HFC 134a and HCFC 123 in a horizontal smooth tube (1st report), Trans. JSME (B) 60 (1994) 239–244.

[35] X. Quan, P. Cheng, H. Wu, An experimental investigation on pressure drop of steam condensing in silicon microchannels, Int. J. Heat Mass Transfer 51 (2008) 5454–5458.

[36] W. Qu, I. Mudawar, Measurement and prediction of pressure drop in two-phase micro-channel heat sinks, Int. J. Heat Mass Transfer 46 (2003) 2737–2753.

[37] H.M. Soliman, The mist-annular transition during condensation and its influence on the heat transfer mechanism, Int. J. Multiphase Flow 12 (1986) 277–288.

[38] A. Cavallini, G. Censi, D.D. Col, L. Doretti, G.A. Longo, L. Rossetto, Condensation of halogenated refrigerants inside smooth tubes, HVAC&R Research 8 (2002) 429–451.